Abstract

The lunar surface consists of a regolith layer that covers the underlying bedrocks, and is generally characterized by particulates <1 cm. The lunar soil is the fine fraction of the regolith, and is generally between 60 and 80 μm. Sizes <10 μm, that comprises ca. 5-20% of the soil, were recognized and petrologically classified.

The coarsest sizes of the regolith are chemically and mineralogically similar, while the finest fractions are more feldspathic, probably due to the easy of fracturing of plagioclase with respect to mafic minerals.

Due to the more feldspathic nature of the very fine lunar soils, in this paper, we quantitatively investigate the influence of very fine (<10 μm) plagioclase on the absorption bands of mafic minerals using the Modified Gaussian Model. We considered two plagioclases with different iron content and two mafic end-members (1) 56% orthopyroxene and 44% clinopyroxene, and (2) 30% orthopyroxene and 70% olivine. We also compared our results with the deconvolution of the same mixtures at coarser sizes. Our results mainly show that:

(1) a fine size acts principally on the reflectance and on the spectral contrast (that increases and decreases, respectively); (2) a very fine plagioclase has a blue slope in the Near Infrared and very shallow 1250 nm band depth, close to zero; (3) consequently, plagioclase band is always shallower than mafic bands; (4) in mixtures with olivine, the composite band center always shows the typical olivine value, differently from coarser mixtures; and (5) mafic material have a blue slope in the Short Wavelength Infrared Region, a more V-shaped 1μm pyroxene absorption and the 1μm mafic band centers are shifted of ca. 40 nm with respect to coarse sizes, reflecting a different weight within the crystal field absorption of mafic component in very fine size. We also evidenced how a coarse plagioclase could be overestimated, while a very fine one could be underestimated if compared to the 63-125μm size.

1. Introduction

Very fine sizes dominate many planetary surfaces and their regolith, e.g., Moon, Mars and Mercury. Different particle size fractions in the regolith (such as soil and dust) affect in different ways the optical properties of the surface. For this reason, very fine particles and their effects on the reflectance spectra of the most common planetary minerals have to be investigated in detail to retrieve correct information about the mineralogical composition and the surface texture.

In particular, the lunar surface consists of a regolith layer that covers the underlying bedrocks, with the exception of steep-sided crater walls, central peaks and lava channels (McKay et al., 1970), as shown by the lunar landings and observations. The lunar regolith, due to the absence of atmosphere on the Moon, is the result of different processes, e.g., impact of meteoroids and bombardments of protons from the sun and the stars, and is generally considered to be characterized by material lower than1 cm in size (McKay et al., 1970). The fine fraction of the regolith, deriving from mechanical disintegration of lunar rocks, both basaltic and anorthositic, constitutes the lunar soil. The average lunar soil size is generally between 60 and 80 μm (McKay et al., 1970). The lunar dust describes even finer material than lunar soils (ca. <50 μm). Furthermore, sizes <10 μm, that comprises ca. 5-20% of the soil, have been recognized and petrologically classified (Laul et al., 1978; 1979; 1980).

Silicate minerals, such as orthopyroxene (OPX), clinopyroxene (CPX), olivine (OL) and plagioclase (PL) are the most important constituents of the lunar surface, associated with oxides (e.g., Papike et al., 1991), and can be spectrally identified on the basis of their absorption bands. While the iron-richer mafic minerals have been always easily detected (e.g., Tompkins and Pieters, 1999; Spudis et al., 1984), only recently, and thanks to the improvements on spectrometers onboard the last missions, the absorption due to the low amount of Fe^{2+} in PL have been recognized (e.g., Ohtake et al., 2009; Cheek et al., 2012a,b; Kramer et al., 2014), permitting new evaluation of its modal abundance and composition.

While coarse sizes of the regolith are chemically and mineralogically very similar, the finest fractions, <10 μm, are different and more feldspathic. A possible explanation can be due to simple comminution processes and the easy of fracturing of PL with respect to mafic minerals (Laul et al., 1978; 1979; 1980; Devine et al., 1982).

According to the more feldspathic nature of the very fine lunar soils, in this paper we present results for a set of PL-bearing mixtures analyzed at the <10 μm particle size, also proposing a comparison with coarser mixtures analyzed in Serventi et al. (2013; 2015), to investigate the effects of very fine sizes on the reflectance spectroscopy of lunar-like mineralogies.

2. Background

2.1 PL and PL-bearing mixtures

Only in the last decade, PL and PL-bearing mixtures have been studied in detail, since the improvements in terms of spectral resolution of the spectrometers onboard the lunar missions permitted to clearly recognize the PL absorption band at ca. 1250 nm due to Fe^{2+} transition in its crystal structure (Adams and Goulland, 1978; Burns, 1993).

Cheek et al. (2011) demonstrated how in a set of synthetic An_{85} PL with different iron content, the 1250 nm band deepens with increasing the iron content, till a maximum value (ca. 0.4 wt.% FeO) after which band depth remains quite constant.

Serventi et al. (2013; 2015) showed that PL could be easily recognized in mixtures with pyroxenes (PX) for modal abundance higher than 70%, while in mixtures with OL it can be masked due to the narrow spectral range in which both OL and PL absorb creating a complex, composite (COMP) absorption. Moreover, spectral parameters, Gaussian modeling and Hapke modeling show how PL can spectrally influence the absorption of mafic minerals (Serventi et al., 2013; 2015; Carli et al., 2014a).

Cheek and Pieters (2014) analyzed PL-rich mixtures with varying content and composition of OL, PX and very high-Mg spinels and demonstrated that PL can significantly contribute to reflectance spectra if strongly absorbing minerals are present in low abundances, particularly in mixtures with PX. Serventi et al. (2016) concluded that, in PL-dominated mixtures: 1) PL can be an important contributor to reflectance spectroscopy also affecting mafic mineral absorption bands (as also demonstrated by Cheek and Pieters, 2014); 2) PL absorbs in the 1250 nm spectral region but iron-rich PL also affects the longest wavelengths (1600-1800 nm), as also suggested by Pieters (1986) and Hiroi et al. (2012); and 3) PX are easily recognizable in mixtures with PL even for very low PX concentration (~1%), while OL, if less than 5%, can be masked by iron-rich PL.

2.2 Particle size

Generally, varying the particle size affects albedo, reflectance and spectral contrast; in particular, decreasing the particle size the albedo increases while the spectral contrast, intended as the strength of the absorptions, is reduced due to the decrease in the mean optical path length of reflected light (Adams, 1968; Pieters, 1983). On the other hand, band centers and band widths are almost unaffected by different particle size (Nash and Conel, 1974), or with shifts that fall in the spectral resolution of the instruments (Serventi et al., 2013).

Crown and Pieters (1987) evaluated the reflectance spectra of mixtures composed with different modal abundance of labradorite (An_{80} PL) and enstatite (Mg-OPX) at different particle size. The authors showed that in the spectra of both end-members and mixtures the reflectance increases while the spectral contrast decreases with reducing the size. In addition, they pointed out how the amount of PL detectable in mixtures with mafic minerals is particle size dependable: more PL is required in finer mixtures.

Mustard and Hays (1997) investigated the effects of fine particles that are approximately the same size as the wavelength of light on reflectance spectra of OL and quartz (in the 0.3-25 μm spectral range). In particular, spectra exhibit a drop in reflectance with the finest sizes. Looking at their Fig. 4, in the 300-2500 nm range, OL albedo increases with fining the size, while the spectral contrast is reduced. Furthermore, the slope in the NIR is less red with decreasing the size. On the contrary, looking at their Fig. 5, quartz's albedo does not change linearly with the particle size; however, the broad absorption at ca. 1000-3000 nm disappears at very fine sizes.

Furthermore, the transparency features show several important changes with decreasing particle size: the spectral contrast increases then decreases, the position of the maximum reflectance of the transparency features shifts systematically to shorter wavelengths, and the symmetry of the features changes.

Cooper and Mustard (1999), analyzing martian analog minerals (e.g., montmorillonite and palagonite), concluded that extremely fine particle sizes generate significant decreases in band strength. In particular, the < 5 μm fractions show vibrational absorption bands that were half the strength of the absorptions from the coarser size fractions. They also concluded that this reduction is due to changes in the ratio of scattering to absorption with particle size, with important implications for the spectroscopic determination of the composition of the extremely fine martian dust.

Craig et al. (2007) evidenced how, increasing particle size, the overall reflectance of OL, OPX and basalts decreases, while the bands deepen to reach a maximum between 45 and 250 μm to then decrease. Coarsening the particle size can also produce band saturation effects that complicates the determination of the absorption band center.

Serventi et al. (2013; 2015; 2016) showed how different particle sizes (125-250 μm; 63-125 μm; 36-63 μm) of PX, OL and PL spectra does not affect the band center (shifts of few nanometers fall in the instrumental resolution) but only the band depth, that decreases decreasing the particle size.

3. Experimental procedure: sample preparation and analytical methods

3.1 End-member preparation and characteristics

Separate end-member minerals were obtained from samples belonging to the Stillwater Complex layered intrusion. The samples were accurately investigated under thin section to evidence the rock mineral association and to reduce as much as possible altered samples (Carli et al., 2009). Among the different samples, we selected an anorthosite, a gabbronorite and an ultramafic rock (for the composition refer to Tab. 1). The chemistry of the rock-forming minerals was determined by electron microprobe analyses with a CAMECA SX50 (EMP) at the microprobe laboratory of C.N.R.-IGG (Consiglio Nazionale delle Ricerche, Istituto di Geoscienze e Georisorse), Padova.

The selected rock samples were first crushed to a coarse size class <2.00 mm, in order to preserve the original rock composition in powdered samples. The powders were then quartered and each fraction was ground to smaller size classes. In particular, we have considered two particle-sizes, <250 μm and <125 μm. Each powder particle-size class was then quartered again and half material was then sieved into two size ranges: 63-125 μm and 125-250 μm. The size fractions have been produced by dry sieving; we decided not to perform wet sieving to avoid: 1) possible alteration or contamination; 2) leaching which can settle the size distribution of our samples, differently from what expected in atmospherless planetary conditions.

From these samples, two PLs with different iron content and two different mafic, multimineralic compositions were separated using a Frantz Isodynamic Magnetic Separator at the Department of Chemistry, Life Sciences and Environmental Sustainability, University of Parma. In Tab. 1, the applied amperage, removed minerals and new samples obtained after magnetic separation are shown. The purity of the end-members has been determined by optical means (X-ray diffraction has been rejected since it is not accurate for phase abundance less than 5%).

167 The selected PL phases include a medium-iron (PL2) and an iron-rich (PL3) PL (both An_{80}, with 0.36
168 and 0.5 wt. % FeO, respectively), while the Fe, Mg (mafic) compositions consist of two distinct
169 mineral assemblages, one PX-bearing (E1), and one OL-rich and PX-poor (E3). The Fe, Mg phases
170 were also analyzed by Mössbauer spectroscopy in order to have a better comprehension of the iron
171 oxidation state (for further details, please refer to Serventi et al., 2013). Fitting of Mössbauer results
172 showed the absence of additional phases.
173
174 **3.2 Mixture preparation**
175 Mixtures of Fe, Mg (E1, E3) and PL (PL2, PL3) end-members were prepared at two different particle
176 sizes (63-125 and 125-250 μm). For each particle size, contents ranging between 20-90 wt. % of each
177 PL end-member was added to each Fe, Mg end-member.
178 For each of the resulting mixtures, we calculated the vol. FeO% due to PL phase with respect to the
179 mixture. The volumetric FeO% is calculated as the FeO wt. % content in PL multiplied by modal PL
180 (%) in each mixture. All the results presented in this work are plotted vs. the vol. FeO in PL.
181 Starting from the 63-125 μm mixtures and end-members, very fine sizes (<10 μm) were produced
182 using a micronizer at the Department of Geosciences, Padova. Each powder, with the addition of water
183 to prevent the heating of the sample, was micronized for 5 minutes; the very fine powder plus water
184 was mixed with ethanol and kept in stove for ca. 2 weeks, until all the water, and ethanol, evaporated.
185 Then, the very fine powders were weighed to check that no loss of material happened during the
186 mechanical grinding.
187
188 **3.3 Spectral measurements**
189 Bidirectional reflectance spectra of each mixture were acquired at room temperature and normal
190 atmospheric pressure with a Field-Pro Spectrometer ® mounted on a goniometer (Istituto di Astrofisica

191 e Planetologia Spaziali, Inaf-IAPS, Roma). The spectra were acquired with a spectral resolution of ~3
192 nm in the VIS and of ~10-12 nm in the NIR and spectral sampling of 1 nm, with *i=30°* and *e=0°*. The
193 source used was a QTH (Quartz Tungsten Halogen) lamp and the spot illuminated has an area of ca.
194 0.5cm^2. The calibration of the spectrometer was performed with Spectralon® optical standard
195 (registered trademark of Labsphere, Inc.).
196 Ten spectra were acquired for each powder, emptying and refilling the cup each time, and then only the
197 mean spectrum was considered for subsequent analyses. In order to avoid problems due to a pressed
198 surface with a "slab-like behavior" or to coarser powder roughness due to the aggregation of such fine
199 particles, powders were gently shaken and pressed in the sample holder.
200 Fig. 1 shows the end-member spectra; mixture spectra are plotted in Fig. 2 and 3, while the continuum-
201 removed spectra of end-members and mixtures are reported in Fig. 4. As a comparison, reflectance
202 spectra of coarser sizes (63-125 μm and 125-250 μm) are shown in Fig. 2,3.
203
204 **3.4 MGM deconvolution**
205 Each spectrum was analyzed applying the Modified Gaussian Model (MGM) algorithm (Sunshine et
206 al., 1990). Briefly, we considered a fixed continuum tangent to the spectrum reflectance maxima as
207 more reliable in the description of the spectrum shape and for modeling the strength of the absorption
208 bands (approach already followed in Clenet et al., 2011 and Serventi et al., 2015).
209 We first deconvolved the end-members, mafic and PL, as mineralogically unknown end-members,
210 assigning Gaussians only where either an absorption band or a band asymmetry are visually perceptible
211 (e.g., 900 nm band in E1 is asymmetric towards the Near Infrared, NIR, region). Then, we deconvolved
212 the mixtures:

1) fixing band center and band width assigned to the mafic end-member absorption bands, with the exception of 1800-2000 nm absoprtion band width that become visually narrower with increasing PL;
2) leaving free the mafic band depth, which depends on mineral abundance in a mixture (e.g. Sunshine and Pieters, 1993; Serventi et al., 2015), and Gaussian parameters assigned to the 1250 nm absorption band (for further details, interested readers are referred to Serventi et al., 2015).

A visual check of the residuals after the fitting, evidenced a pattern in the 700-1100 nm spectral range of the E1-bearing mixtures not detected at coarser sizes. For this reason, starting from values obtained from the fit with the procedure described above, we recomputed MGM leaving free the mafic parameters (see Section 4.3).

A number was assigned to each Gaussian, as described in Tab.2.

4. Results

4.1 End-member and mixture reflectance spectroscopy

A comparison between the end-members is plotted in Fig. 1. In particular, considering the very fine size, (1) PL spectra (Fig. 1a,b) are characterized by a blue slope in the NIR and are almost featureless; (2) E1 900 nm band becomes V-shaped (Fig. 1c) and the band asymmetry towards the NIR is emphasized. This asymmetry seems to be correlated to a shift of the 900 nm band towards shorter wavelengths, as if, with decreasing the size, OPX becomes even more dominant than CPX; (3) the E3 complex 1050 nm band (Fig. 1d) is characterized by three multiple absorptions due to the Fe^{2+} transitions in OL M1 and M2 sites, but the absorption centered at ca. 1250 nm seems shallower with respect to coarser sizes; (4) mafic assemblages (Fig. 1c,d) show a more marked blue slope in the short

236 wavelength infrared region (SWIR) with respect to the coarsest size, and (5) E3 (Fig. 1d) shows the
237 appearance of an evident absorption at 2000 nm.
238 Both E1 and E3 indicate more influencing OPX reflectance properties with respect to other mafic
239 phases such as OL, CPX. However, the rock sample from which E3 was magnetically separated
240 contains 2% of chromite. Even if the residual chromite in our sample after separation is very low
241 (<<0.5%), chromite is characterized by a deep absorption at ca. 2000 (e.g. Cloutis et al., 2004), and,
242 thus, we cannot completely rule out chromite as a contributor to the 2000 nm absorption.
243 PL end-members were magnetically separated from rocks containing PX. The separated PL was
244 investigated by optical microscope analysis with no detection of residual PX, but we have to consider
245 that PX inclusions could still be present. For this reason, the 900 nm band showed by PL spectra in Fig.
246 1a could be indicative of residual PX. Furthermore, Fig. 1b reveals how a fine size emphasizes the
247 effects of residual PX; the 900 nm band due to Fe^{2+} in PX becomes more absorbing with decreasing the
248 size (see also the continuum-removed spectrum in Fig. 4b).
249 Fig. 2, 3 show that a fine particle size (Fig. 2a, b and Fig. 3a, b) increases the reflectance and reduces
250 the spectral contrast compared to the coarsest sizes (Fig. 2c-f and Fig. 3c-f).
251 Considering the 63-125 and 125-250 μm sizes (Fig. 2c-f, 3c-f), a higher PL modal abundance results in
252 a systematic increase of the reflectance, whereas in the <10 μm size some spectra deviate from this
253 behavior, such as the 70%PL3-E3 and the PL end-members (see Fig. 2a,b, 3a,b). As explained in
254 Section 3., working with such fine sizes means to deal with problems due to too much pressed surfaces
255 or to a powder roughness. For this reason, spectra acquired on the same sample have variable
256 reflectance values, with the mean spectrum showing a standard deviation up to ca. 6% that can explain
257 the reflectance non-linear behavior with increasing PL modal abundance.
258 PL in very fine E1-bearing mixtures results in a weaker absorption band with respect to the coarse sizes
259 and is revealed by a flattening in the 1200 nm spectral region for 80% PL-mixture (Fig. 4a,b). A weak

absorption band can be recognize only for more than 90% PL (light-grey spectra in Fig. 4a,b), but always shallower than PX absorption bands.

Serventi et al. (2013) demonstrated how the spectral parameters describing the COMP band, due to the simultaneous absorptions of OL and PL, give information on the relative minerals' modal abundance. In particular, considering coarse E3-bearing mixtures, the COMP band center shifts from typical OL values (1050 nm) to PL values (1250 nm) for PL content >70% (see their Fig.13b). However, investigating the < 10 μm size, the center shifting is not detectable (Fig. 4c,d); this is consistent with the featureless nature of PL.

4.2 End-member deconvolution

End-members were deconvolved via MGM (see Fig. 5a, 6a; to show the goodness of the fit, RMS is plotted). E1 residual (Fig. 5a, h) shows a sinusoidal pattern in the 700-1100 nm; comparing our residuals with those from Klima et al. (2008), which showed the same pattern and the same RMS as ours, we decided not to add additional Gaussians.

A comparison with the deconvolution of coarser sizes (see Tab. 3) demonstrates how the 900-1000 nm absorptions are fitted with the same number of Gaussians, with the only exception of E1, where an adjustment Gaussian (G5) centered at ca. 840 nm is not here introduced (in accordance with Klima et al., 2007). Despite end-member residual seems to indicate a sinusoidal pattern, covariance matrix does not allow to add more Gaussians. Moreover, a similar residual pattern is present also in Klima et al. (2007) and Klima et al. (2011). On the contrary, G5 is required for coarser size as discussed in Serventi et al. (2015; 2016) and in accordance with Sunshine and Pieters (1993).

To summarize, Tab. 3 shows how reducing the particle size (i.e., from 250 to 10 μm) of E1:

1) As aforementioned, G5 is not needed;

2) Bands are shallower, above all G1 and G3, and the Gaussians describing the different absorption bands are very similar in terms of band depth, thus reflecting the general spectral contrast;
3) G1 and G2 centers shift towards shorter wavelengths (more than 40 nm);
4) The 1850 nm absorption is fitted with only one Gaussian (G3); and
5) Band widths do not show significant changes.

Considering E3, a reduced size produces shallower bands, and a narrower G8 with respect to coarse ones; G6-G8 centers shift towards longer wavelengths, but with reduced shifts compared to E1. G7 is the deepest one and this is not consistent with the results by Sunshine and Pieters (1998), where G8 is the deepest. However, Buz and Ehlmann (2014) demonstrated how extreme size values may affect the OL spectral parameters that, consequently, deviate from the trend found by Sunshine and Pieters (1998). The authors showed how at very fine sizes (<45 μm) G7 is the deepest Gaussian, also in accordance with results from Burns (1993). However, considering E3 (Fig. 6a), G6 is slightly deeper than the results by Buz and Ehlmann (2014), but here we are dealing with even finer sizes. Furthermore, the OPX component may influence G6 depth.

The longest wavelengths of E3 are deconvolved with a Gaussian at 1963 nm that can be tentatively assigned either to PX or to chromite (Fig. 6a; Tab. 3).

Tab. 4 reports the PL end-member spectral parameters after MGM deconvolution for the different particle sizes. MGM fits are also shown in Fig. 5g,n. In particular, reducing the size, the 1250 nm absorption can still be considered, even if for the finest size the band depth is close to zero. The band center shifts towards longer wavelengths both for PL2 and PL3, even if with shifts less than 10 nm. Tab. 4 shows how a coarse PL2 is deeper than the iron-richer PL3 (also refer to Serventi et al., 2015; 2016); however, the <10 μm PL3 is deeper than PL2. This can be related to the residual PX in PL2 (after magnetic separation is estimated to be less than 1%) that at very fine sizes becomes spectrally

307 important, thus influencing and reducing the PL band depth. Furthermore, the residual PX produces a
308 900 nm absorption band that is only slightly less deep than the PL absorption band (0.015 vs. 0.026 -
309 LnRefl, also see Fig. 3a). The 900 nm band depth in PL3, not detectable at the coarser sizes, represents
310 the 30% of the <10 μm PL band depth (see Tab. 4), a further demonstration of the featureless behavior
311 of fine PL.
312 G11, that in literature (e.g., Pieters, 1996; Hiroi, 2012; Serventi et al., 2015; 2016) was tentatively
313 attributed to PL, at the <10 μm size is shallower, shifted towards longer wavelengths (1940-1950 nm)
314 and narrower with respect to the coarse sizes. Consequently, in this case, G11 probably adjusts the
315 vibrational processes related to the OH^- alterations of the natural PL here considered.
316
317 **4.3 Mixture deconvolution**
318 Mixtures were deconvolved following the procedure described in Section 3. Fitting results, as well as
319 RMS, are shown in Fig. 5, 6.
320 PL band slightly deepens in E1 mixtures (triangles in Fig. 7a), while COMP band decreases in E3
321 mixtures (stars in Fig. 7a). In Fig. 7b, PL and COMP band center shifts towards longer wavelengths
322 with increasing the vol. FeO% in PL. Both PL (triangles in Fig. 7c) and COMP (stars in Fig. 7c) band
323 widen with increasing vol. FeO% values in mixtures.
324 Fig. 8a,b show that increasing the vol. FeO% in PL, the Gaussians describing the mafic absorptions
325 become shallower. Fig. 8a displays in detail the behavior described in Section 4.1, with mafic
326 absorption bands deeper in 60%PL2-E1 and in 80%PL2-E1 than in 50%PL2-E1 and 70% Pl2-E1,
327 respectively. However, we report the error bar for band depth, calculated in the 95% confidence
328 interval, and it is clear how 50%PL2-E1 has a much larger error bar than 60%PL2-E1 (±0.05LnRefl
329 with respect to ±0.015LnRefl). Fig. 7b shows how the depth of Gaussians describing the mafic
330 absorptions in E3-bearing mixtures decreases more linearly than E1-mixtures.

As stated in Section 3.4, the mafic parameters, with the exception of the depth, has been kept fixed in the first iteration. Basing on the residuals, we decided to leave free those parameters. Their variations have been reported in Fig. 8b,c and in Fig. 8e, for E1 and E3-bearing mixtures, respectively. Fig. 8b shows that G1 and G2 move towards longer wavelengths with increasing PL modal abundances; however, G1 variations for <90% PL and G2 variations for <80% PL are less 10 nm, respectively, and, so within the instrumental spectral resolution. On the contrary, G1 and G2 shift towards longer wavelengths of 12 nm (90% PL), and of 20 nm (80% PL) and 40 nm (90% PL), respectively. These values, in particular for G2, cannot be justified by the spectral resolution but must be related to the presence of PL which is not only accommodate by G10 and G11. Fig. 8c reports how G3 becomes narrower with increasing PL modal abundances, while G2 varies slightly only for PL more than 80%. G3 variations can be related to PL.

Regarding E3-bearing mixtures (see Fig. 8e), only G3 width varies: G3 becomes narrower with increasing the PL content (with no differences between PL2 and PL3-bearing mixtures, as the values lay on the bisector line), with substantial variations for mixture with more than 70% PL.

Fig. 9 shows a comparison for the spectral parameters after MGM deconvolution for the three different particle sizes: <10 μm (pink and violet symbols, for PL2 and PL3-bearing mixtures, respectively), 63-125 μm (light-blue and blue symbols for PL2 and PL3-bearing mixtures, respectively) and 125-250 μm (yellow and red symbols for PL2 and PL3-bearing mixtures, respectively). As already stated in section 2.3, the principal difference regards the band depth; Fig. 9a,d evidence how PL and COMP band are shallower compared to coarser sizes , with depth close to zero. In addition, the band width in the fine particle size is strongly reduced (Fig. 9c,f), particularly in E3-bearing mixtures.

5. Discussions

In this paper we investigated the effects of a very fine particle size on the reflectance spectroscopy of PL, mafic end-members and PL-bearing mixtures.

As already stated by Adams (1968) and Pieters (1983), a fine particle size increases the reflectance and decreases the spectral contrast. Mustard and Hayes (1997) also evidenced how, fining the size, OL becomes brighter but shallower, and bluer in the NIR (see their Fig. 4A).

In this work, we also showed how the spectra of very fine PL become featureless, with a bluer slope than a coarse PL in the IR, and how the difference in reflectance between mixtures and end-members is reduced. Consequently, the general reflectance's increase with increasing the PL abundance documented at coarser sizes, may not be always respected. This behavior, as well as the bluer slope towards the IR, similar to what happens in bulk surfaces of rocks spectra (as also postulated by Harloff and Arnold, 2001, Pompilio et al., 2007; Carli, 2009), clearly demonstrates how a very fine size could complicate the interpretation of a reflectance spectrum (e.g., slope similar for very fine size and slab of rocks), as well as the evaluation of the minerals' modal abundance.

Cheek and Pieters (2014) and Serventi et al. (2015, 2016) demonstrated how, considering PL-dominated mixtures (PL>70/80%), Fe^{2+}-bearing PL can significantly contribute to reflectance spectra, also affecting mafic mineral absorption bands. In fact, in PX-bearing mixtures PL absorption band is even deeper than PX bands for very high PL content, while, in OL-bearing mixtures, the COMP band position shifts towards the typical PL center values (1250-1300 nm) for high PL content. All these effects are stronger in the 125-250 μm size than in 63-125 μm one, thus supporting that a coarse PL is spectroscopically more active than a fine one. On the contrary, this work evidences the unpredictable effects of a very fine size on reflectance spectroscopy. For example, the band depth of a very fine PL is very shallow, with a Gaussian depth almost close to zero, and the COMP band center always shows the typical OL values, even for PL>90%. This testifies how a reduced size can mask the contribution of PL

on reflectance spectra, with a consequent and possible PL underestimation, that, obviously, leads to mistakes in the interpretation of reflectance spectra from a Solar System body's surface.

Furthermore, we suppose that the 1800 nm absorption detected at coarse sizes may be not effective at such fine size. In the very fine PL considered in this work, G11 is narrower and shifted towards longer wavelengths (1940-1950 nm) with respect to the coarse sizes and, therefore, probably related to the OH^- alteration of the terrestrial PL.

Here, we introduce an index called Band Depth Ratio (B.D.R.) calculated as follow:

$$B.D.R.(E1) = \frac{B.D.\,G10}{B.D.\,G10 + B.D.\,G1 + B.D.\,G2} \quad [1]$$

$$B.D.R.(E3) = \frac{B.D.\,G9}{B.D.\,G9 + B.D.\,G6 + B.D.\,G7} \quad [2]$$

Where B.D. is the band depth of each Gaussian. This index returns the relative intensity of PL and COMP bands with respect to all the Gaussians describing the 1000 nm absorption.

We calculated B.D.R. (E1, E3) for <10, and 63-125 and 125-250 μm (Serventi et al., 2015) sizes. Results are plotted vs. the 63-125 μm size (Fig. 10); the bisector indicates the ideal conditions that the relative depths do not change with the size. However, symbols do not lay on the bisector: 125-250 μm values (blue symbols) stay in general slightly above the line, while <10 μm values (magenta symbols) are under the line. This demonstrates that, considering the 63-125 μm size as a reference, coarse PL can be slightly overestimated, and very fine PL could be easily underestimated. Moreover, increasing the PL abundance generally increases also the difference between B.D.R. for <10 μm and for 63-125 μm.

The spectral properties of mafic end-members are affected by very fine sizes too. Regarding E1, the 900 nm absorption band is more V-shaped, asymmetric towards the NIR with respect to the coarse sizes and shifted towards shorter wavelengths , thus simulating different mineral content and/or different mineral chemistry (shorter wavelengths correspond to Mg-richer and Ca-poorer PX). The very

399 fine E1 deconvolution does not require G5, on the contrary needed for coarser sizes (see also Pieters et
400 al., 1993; Serventi et al., 2013).
401 On the other hand, the fine E3 end-member shows two main differences if compared to coarser sizes.
402 The G6-G8 relative depths are not consistent with the trend proposed by Sunshine et al. (1998),
403 confirming the unpredictable effects of very fine sizes; in fact, Buz and Ehlmann (2014) demonstrated
404 how extreme sizes affect the spectral parameters of OL. Furthermore, the fine E3 longest wavelengths
405 show an absorption not detected at coarser sizes. Since E3 is characterized by 70% of OL and 30% of
406 OPX, it seems plausible that at very fine size the presence of OPX, not detectable at coarser sizes,
407 could become an important spectroscopic contributor.
408 The spectral properties seen in E1 (band center shifting) together with the behavior seen for E3 in the
409 longest wavelengths, seem to evidence how OPX spectrally dominates at such fine size with respect to
410 other, mafic phases, which present a lower amount of total iron. However, E3 band can be related to
411 residual chromite after magnetic separation.
412 Comparing 63-125 μm and 125-250 μm sizes, Gaussians shift less than 10 nm. The FieldSpec spectral
413 resolution varies between 2 and 12 nm: thus, the band center shifting falls in the instrumental
414 resolution. On the contrary, mafic band centers for <10 μm powders are shifted of ca. 40 nm with
415 respect to the coarser sizes; this is because we are dealing with sizes that are approximately the same
416 size as the wavelength of light and this could lead to unexpected behaviors of the spectral parameters.
417 Fig. 11 reports spectra of lunar soils (from the Lunar Soil Characterization Consortium, Pieters et al.,
418 1993; 2000) at three different fine to very fine particle sizes (20-45μm blue spectra, 10-20μm red
419 spectra and <10μm black spectra) acquired from the Apollo missions 14 and 16. In particular, samples
420 #67481 and #67461 are more enriched in PL than samples #14141 and #62231. Generally, reducing the
421 size the reflectance increases. As expected, absorption bands are shallower and, in particular, the 1250
422 nm weak band becomes almost featureless in <10 μm spectra. Furthermore, Fig.11 emphasizes the

behavior of the <10 μm fractions: spectral contrast is extremely reduced if compared to the 10-20 μm size. Anyway, we have to take into account that spectra of lunar samples are affected by the presence of npFe° due to the space weathering, which implies a red slope and lower albedo than expected for PL-rich fine powders. Nevertheless, the spectra from lunar soils are in accordance with a relative increase in albedo and a strong reduction in absorptions reducing the size and an almost featureless spectrum for <10 μm size, loosing information about PL absorption.

Generally, the main feature that discriminates the very fine size is the high albedo, correlated with the decreasing absorption intensity. However, due to the space weathering, this feature may not be so easily recognized on lunar spectra. The low spectral contrast could be evidence of very fine size as well; however, a fine size is not the only reason to explain reduce contrasts (e.g., space weathering, shock effects).

6. Conclusion and implications for the Moon

The Moon regolith, generally <1 cm in size, comprises the lunar soil, which represents the finest fraction of the regolith and derives from mechanical disintegration of lunar rocks, both basaltic and anorthositic, and is generally between 60 and 80 μm. Very fine sizes (<10 μm) were recognized and thought to represent the 5-20% of the lunar regolith; PL is the dominant phase of this fine regolith (Laul et al., 1978; 1979; 1980).

In this work, we demonstrated how a very reduce size implies a higher albedo and a decrease in the spectral contrast, particularly for the PL spectra that become almost featureless. On the other hand, we showed how the iron-richest mineral in the considered mixtures, OPX, seems to spectrally dominate other mafic and cogenetic minerals, CPX and OL, at the very fine size (e.g., the 900 nm band shift towards shorter wavelengths in E1 and the 2000 nm reflectance decrease in E3).

This has important implications for the lunar regolith, where PL is abundant. For example, the presence of PL spectra with a well-defined and deep 1250 nm absorption gives indications not only on the crystallinity of the mineral but also on the particulate size that cannot be too fine in the areas were PL absorption is detected. On the other hand, featureless PL spectra can lead to an erroneous interpretation of the PL abundance, and/or chemistry that can be underestimated. These results evidence that more detailed investigations on such fine sizes should be pursued to better understand how to retrieve composition by modeling remote sensing data.

Acknowledgment

Spectroscopic measurements were carried out at Inaf-IAPS-Istituto Nazionale di Astrofisica, Roma. EMPA analyses and powder micronization have been performed at Dipartimento di Geoscienze, Padova. The authors are grateful to prof. Maria Sgavetti for her thoughtful review that greatly improved the quality of the manuscript. The authors are also grateful to two anonymous reviewer for their stimulating comments and suggestions.

References

Adams, J. B., Goulland, L. H., 1978. Plagioclase feldspar: visible and near infrared diffuse reflectance spectra as applied to remote sensingProc. Lunar Sci. Conf. 3, 2901-2909.

Burns, R.G., 1993. Mineralogical applications of crystal field theory. Cambridge University Press, Cambridge. 551 pp.

Buz, J., Ehlmann, L., 2014. Effects of grain size on the reflectance spectroscopy of olivine in the VIS-NIR and the derivation of olivine composition using modified Gaussian modeling. Lunar. Planet. Sci. 45. Abstract 2810.

469 Carli, C., 2009. Spectral analyses in the VNIR of igneous rocks: Surface composition characterization
470 of terrestrial planets. Plinius 35, 83–90.
471 Carli, C., Ciarniello, M., Capaccioni, F., Serventi, G., Sgavetti, M., 2014a. Spectral variability of
472 plagioclase-mafic mixtures (2): investigation of the optical constant and retrieved mineral
473 abundance dependence on particle size distribution. Icarus, 235, 207-219.
474 Carli, C., Serventi, G., Sgavetti, M.; 2014b. VNIR spectral variability of the igneous stratified
475 Stillwater Complex: a tool to map lunar highlands. Am. Min. 99, 1834-1848
476 Cheek, L. C., Pieters, C.M., Parman, S.W., Dyar, M.D., Speicher, E.A., Cooper, R.F., 2011. Spectral
477 characteristics of PL with variable iron content: application to the remote sensing of the lunar
478 crust. Lunar. Planet. Sci. 42. Abstract 1617.
479 Cheek, L.C., Pieters, C.M., 2012a. Variations in anorthosite purity at Tsiolkovsky crater on the Moon.
480 Lunar. Planet. Sci. 43. Abstract 2624.
481 Cheek, L. C., Donaldson Hanna, K.L., Pieters, C.M., Head, J.W., Whitten, J.L., 2012b. The distribution
482 and mineralogy of anorthosite in the Orientale Basin: new perspective from M^3 data. Second
483 conference on the lunar highland crust. Abstract 9022.
484 Cheek, L. C., Pieters, C. M., 2014. Reflectance spectroscopy of plagioclase-dominated mineral
485 mixtures: implication for characterizing lunar anorthosites remotely. Am. Min., 99, 1871-1892.
486 Cloutis, E.A., Sunshine, J.M., Morris, R.V., 2004. Spectral reflectance-compositional properties of
487 spinels and chromites: Implications for planetary remote sensing and geothermometry.
488 Meteorit. Planet. Sci. 39, 545–565.
489 Cooper, C.D., Mustard, J.F., 1999. Effects of Very Fine Particle Size on Reflectance Spectra of
490 Smectite and Palagonitic Soil. Icarus 142, 557–570

491 Craig, M.A., Cloutis, E.A., Bailey, D.T., 2007. The effects of grain size, <45-1000 μm, on the
492 reflectance spectrum of planetary analogs from 0.35-2.5 μm. Lunar. Planet. Sci. 38. Abstract
493 1356.
494 Crown, D.A., Pieters, C.M., 1987. Spectral properties of PL and pyroxene mixtures and the
495 interpretation of lunar soil spectra. Icarus, 72, 492-506.
496 Devine, J.M., McKay, D.S., Papike, J.J., 1982. Lunar regolith: petrology of the <10 μm fraction. Proc.
497 Lunar Planet Sci. Conf. 13th, A260-A268
498 Harloff, J., Arnold, G., 2001. Near-infrared reflectance spectroscopy for bulk analog materials for
499 planetary crust. Planet. Space Sci., 49, 191-211
500 Hiroi, T., et al. 2012. Diversity in the visible-NIR absorption band characteristics of lunar and
501 asteroidal plagioclase. Lunar. Planet. Sci. 43. Abstract 1168
502 Kramer, G. Y., Kring, D. A., Mahm, A. L., Pieters, C. M., 2013. Spectral and photogeologic mapping
503 of Schrödinger Basin and implications for post-South Pole-Aitken impact deep subsurface
504 stratigraphy. Icarus, 223, 131-148
505 Laul, J.C., Vaniman, D.T., Papike, J.J., Simon, S.B., 1978. Chemistry and petrology of size fractions of
506 Apollo 17 deep drill core 70009-70006. Proc. Lunar Planet Sci. Conf. 9th, 2065-2097
507 Laul, J.C., Lepel, E.A., Vaniman, D.T., Papike, J.J., 1979. The Apollo 17 drill core: chemical systematics
508 of grain size fractions. Proc. Lunar Planet Sci. Conf. 10th, 1269-1298
509 Laul, J.C., Papike, J.J., 1980. The lunar regolith: comparative chemistry of the Apollo sites. Proc. Lunar
510 Planet Sci. Conf. 11th, 1307-1340
511 McKay D. S., Heiken G., Basu A., Blanford G., Simon S., Reedy R., French B. M., and Papike J. (1991)
512 The lunar regolith. In Lunar Sourcebook: A User's Guide to the Moon (G. H. Heiken, D. T.
513 Vaniman, and B. M. French, eds.) Cambridge University Press, Cambridge. 285-356.

514 Mustard, J.F., Hays, J.E., 1997. Effects of hyperfine particles on reflectance spectra from 0.3 to 25 μm.
515 Icarus, 125, 145-163
516 Nash, D.B., Conel, J.E., 1974. Spectral reflectance systematics for mixtures of powdered hypersthene,
517 labradorite, and ilmenite. J. Geophys. Res. 79, 1615-1621.
518 Ohtake, M., et al., 2009. The global distribution of pure anorthosite on the Moon. Nature 461,
519 doi:10.1038/nature08317
520 Papike, J.J., Taylor, L. A., Simon, S., 1991. Lunar minerals, in The Lunar Sourcebook, edited by G.
521 Heiken, D. Vaniman, and B. French, pp. 121 – 181, Cambridge Univ. Press, New York.
522 Pieters, C. M., Fischer, E. M., Rode, O., Basu, A., 1993. Optical effects of space weathering: the role of
523 the finest fraction. J. Geophys. Res., 98, 20,817-20,824.
524 Pieters, C. M., 1996. Plagioclase and maskelynite diagnostic features. Lunar. Planet. Sci. 27, Abstract
525 1031
526 Pieters, C.M., et al., 2000. Space weathering on airless bodies: resolving a mystery with lunar samples.
527 Meteor. Planet. Sci., 35
528 Serventi, G., Carli, C., Sgavetti, M., Ciarniello, M., Capaccioni, F., Pedrazzi, G., 2013. Spectral
529 variability of plagioclase-mafic mixtures (1): effects of chemistry and modal abundance in
530 reflectance spectra of rocks and mineral mixtures. Icarus, 226, 282-298,
531 doi:10.1016/j.icarus.2013.05.041
532 Serventi, G., Carli, C., Sgavetti, M., 2015. Spectral variability of plagioclase-mafic mixtures (3):
533 quantitatively analysis appling the MGM algorithm. Icarus, 254, 34-55,
534 doi:10.1016/j.icarus.2015.03.024
535 Serventi, G., Carli, C., Sgavetti, M., 2016. Deconvolution of mixtures with high plagioclase content for
536 the remote interpretation of lunar plagioclase-rich regions. Icarus, 272, 1-15,
537 doi:10.1016/j.icarus.2016.01.020

538 Spudis, P.D., Hawke, B.R., Lucey, P.G., 1984. Composition of Orientale Basin Deposits and
539 Implications for the Lunar Basin-Forming Process. J. Geophys. Res., Vol. 89, 197-210
540 Sunshine, J.M., Pieters, C.M., Pratt, S.F., 1990. Deconvolution of mineral absorption bands: an
541 improved approach. J. Geophys. Res., Vol. 95, 6955-6966.
542 Sunshine, J.M., Pieters, C. M., 1998. Determining the composition of olivine from reflectance
543 spectroscopy. J. Geophys. Res., Vol. 103, 13675-13688.
544 Tompkins, S., Pieters, C. M., 1999. Mineralogy of the lunar crust: results from Clementine. Meteoritics
545 & Planetary Science, 34, 25-41.
546
547
548 **Figure captions**
549 1) End-member reflectance spectra at three different particles sizes, 125-250 μm (black), 63-125
550 μm (dark gray) and <10 μm (light gray). Generally, reducing the particle sizes the albedo
551 increases and the spectral contrast is reduced. a,b) Very fine PL are characterized by featureless
552 spectra with a blue slope; c) very fine E1 shows a 900 nm band shifted towards shorter
553 wavelengths and more asymmetric towards the NIR with respect to the coarse sizes; and d) the
554 fine E3 complex 1050 nm band is characterized by three multiple absorptions, but the
555 absorption centered at ca. 1250 nm seems shallower with respect to the coarse sizes and is
556 evident the appearance of an absorption at 2000 nm.
557
558 2) Reflectance spectra of E1-PL mixtures at three different particle sizes. a,b) E1+PL2 and
559 E1+PL3, <10 μm; c,d) E1+PL2 and E1+PL3, 63-125 μm; and e,f) E1+PL2 and E1+PL3, 125-
560 250 μm. Generally, a fine particle size produces spectra with higher reflectance and reduced
561 spectral contrast compared to the coarsest sizes.

3) Reflectance spectra of E3-PL mixtures at three different particle sizes. a,b) E3+PL2 and E3+PL3, <10 μm; c,d) E3+PL2 and E3+PL3, 63-125 μm; and e,f) E3+PL2 and E3+PL3, 125-250 μm. Generally, a fine particle size produces spectra with higher reflectance and reduced spectral contrast compared to the coarsest sizes.

4) End-member and mixture continuum-removed reflectance spectra. Generally, increasing the PL content in mixtures, the mafic absorptions are reduced, while the PL band behavior depends on the mafic end-member. a,b) E1-PL2 and E1-Pl3 mixtures, respectively. PL produces an absorption bands only for very high PL content, more than 80%; c,d) E3-PL2 and E3-Pl3, respectively. The COMP band center shifts from typical OL (1050 nm) values to PL (1250 nm) values is not detectable/noticeable.

5) MGM deconvolution and residuals (expressed in terms of Root Mean Square, RMS) of E1-bearing mixtures. RMS values are consistent with Klima et al. (2011). a-g) E1-PL2 mixtures; h-n) E1-PL3 mixtures. Continuum-removed reflectance is expressed as –LnRefl.

6) MGM deconvolution and residuals (expressed in terms of Root Mean Square, RMS) of E3-bearing mixtures. RMS values are consistent with Klima et al. (2011). a-g) E1-PL2 mixtures; h-n) E1-PL3 mixtures. Continuum-removed reflectance is expressed as –LnRefl.

7) The figure shows the spectral parameter variations in mixtures composed with E1/E3 and PL2,3 after MGM deconvolution. In particular, with increasing the volumetric FeO% in PL: a) PL band deepens (triangles), while the COMP band depth decreases (stars); b) PL band center

(triangles) and COMP band center (stars) shift towards longer wavelengths (triangles); and c) both PL (triangles) and COMP band (stars) widen.

8) The figure shows the spectral parameter variations in mixtures composed with E1/E3 and PL2,3 after MGM deconvolution. In particular, with increasing the volumetric FeO% in PL: a,d) the mafic band depth decreases both in E1 and in E3-bearing mixtures. Fig. 8a also shows the vertical error bars for the 50-80% PL2-E1 mixtures; b) G1 and G2 move towards longer wavelengths with increasing PL modal abundances. G1 variations and G2 variations for <80% PL are less than 10 nm and, so, explainable by the instrument spectral resolution; G2 shifts for 80% and 90% PL can be related to the presence of PL; c) G3 become narrower with increasing PL modal abundances, while G2 varies only slightly; only G2 variations for more than 70% PL2 can be related to PL, while other variations are, again, explainable with the instrument spectral resolution; and e) G3 becomes narrower with increasing the PL content (with no differences between PL2 and PL3-bearing mixtures, as the values lay on the bisector line), but variations are substantial only for more than 80% PL.

9) The figure shows a comparison for the spectral parameters after MGM deconvolution for the three different particle sizes: <10 μm (violet symbols), 63-125 μm (pink symbols) and 125-250 μm (fuchsia symbols). a,d) PL (in E1-bearing mixtures) and COMP (in E3-bearing mixtures) band depths are very reduced compared to the coarse sizes and close to zero; b,e) the PL band center does not show great variations in E1-bearing mixtures, while in E3-PL2 mixtures the COMP band center is shifted towards longer wavelengths. On the contrary, is shifted towards shorter wavelength in E3-PL3 mixtures; and c,f) the band width in the fine particle size is strongly reduced, particularly in the E3-bearing mixtures.

10) Band Depth Ratio (B.D.R.) for the 125-250 μm and <10 μm sizes vs. the 63-125 μm size. a) E1-bearing mixtures; b) E3-bearing mixtures. The bisector indicates the ideal conditions that the relative depths do not change with the size; however, 125-250 μm values (blue symbols) stay above the line, while <10 μm values (magenta symbols) are under the line.

11) Spectra of lunar soils (from the Lunar Soil Characterization Consortium, from Pieters et al., 1993; 2000) at three different, very fine particle sizes (20-45μm blue spectra, 10-20μm red spectra and <10μm black spectra). Samples #67481 and #67461 are more enriched in PL than samples #14141 and #62231.Generally, reducing the size the reflectance increases, absorption bands are shallower and, in particular, the 1250 nm band becomes almost featureless in <10 μm spectra.

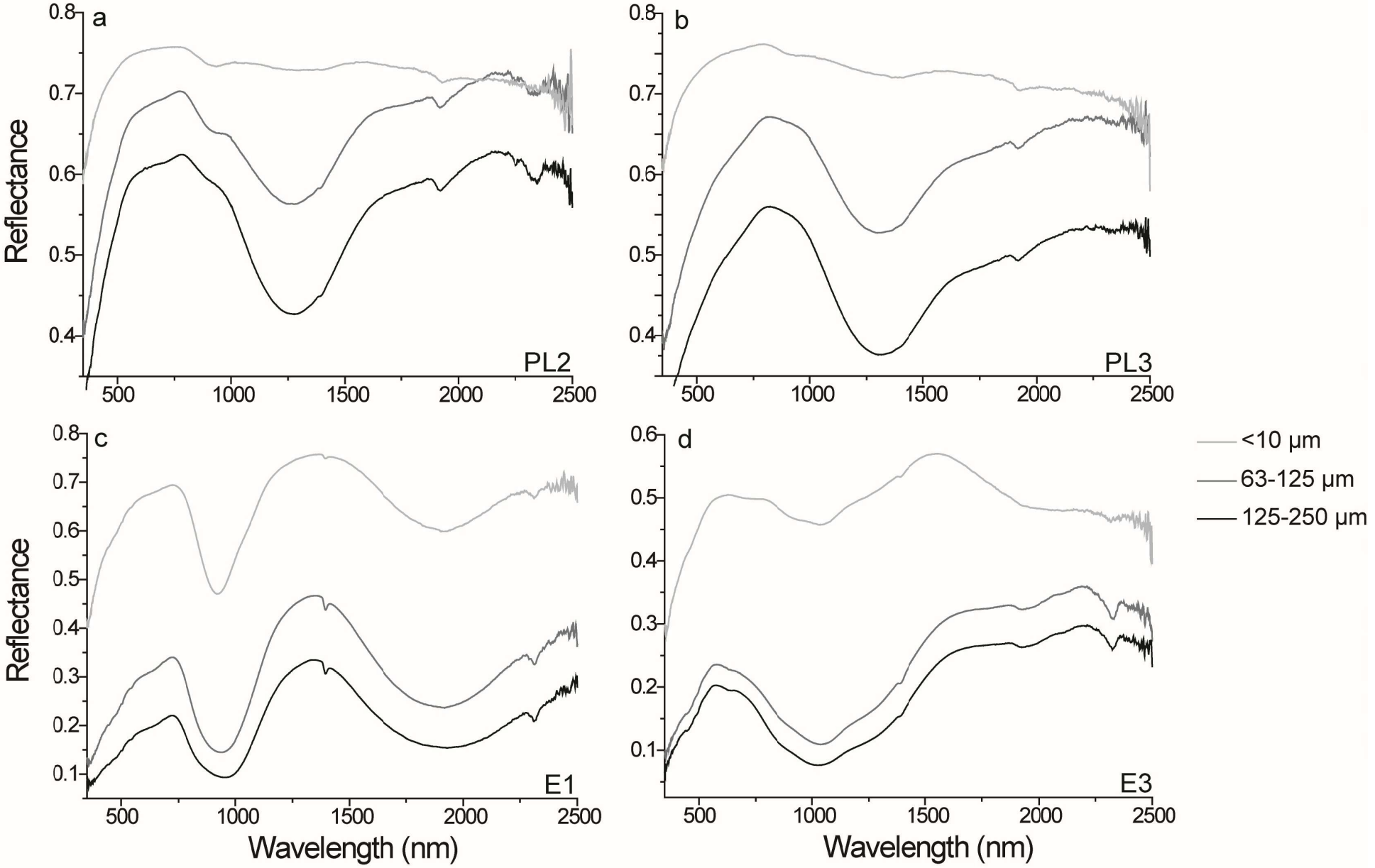
a
b
c
d
PL2
PL3
E1
E3
Reflectance
Wavelength (nm)
<10 µm
63-125 µm
125-250 µm

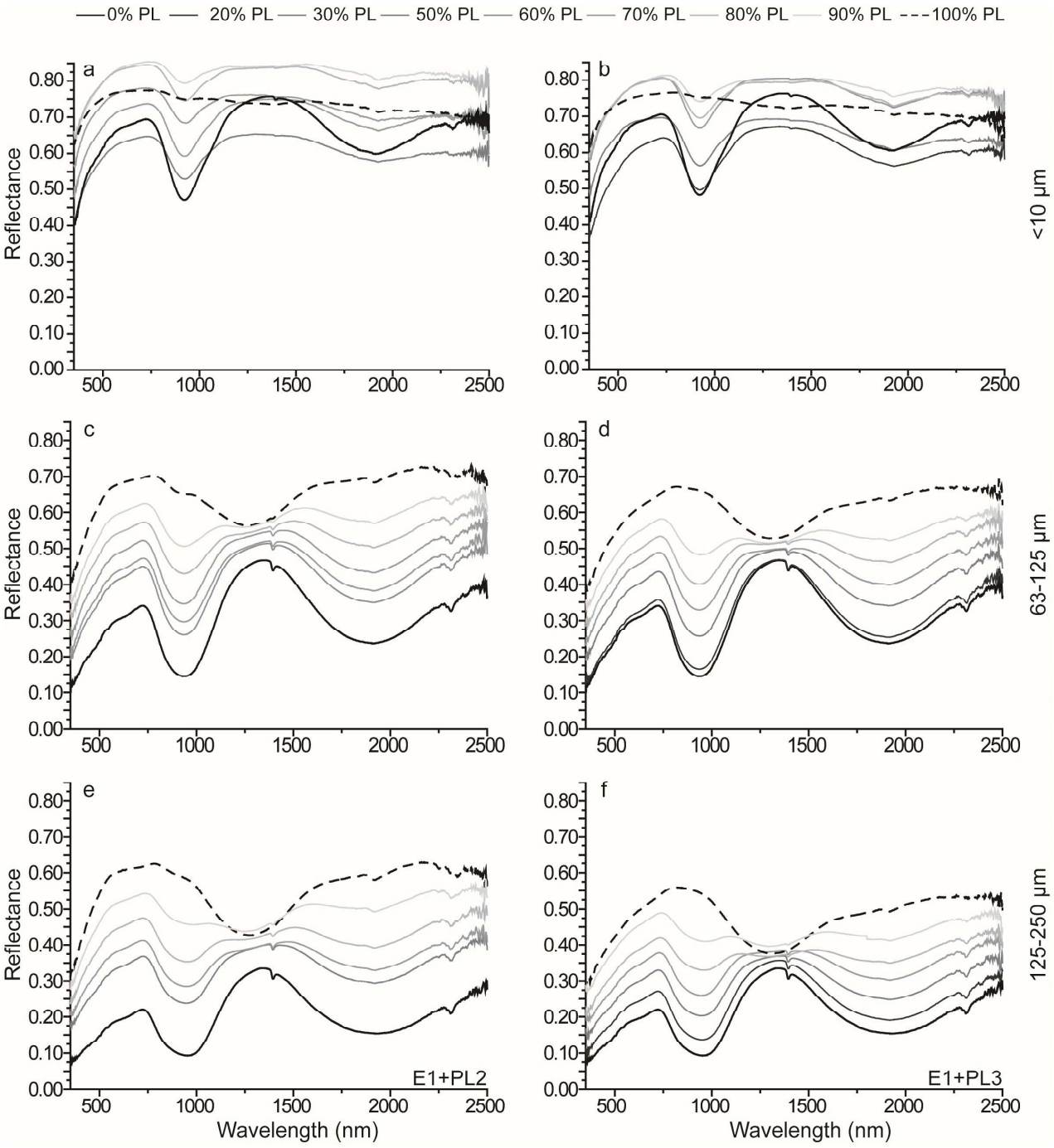
0% PL
20% PL
30% PL
50% PL
60% PL
70% PL
80% PL
90% PL
100% PL
a
b
c
d
e
f
Reflectance
Wavelength (nm)
<10 µm
63-125 µm
125-250 µm
E1+PL2
E1+PL3

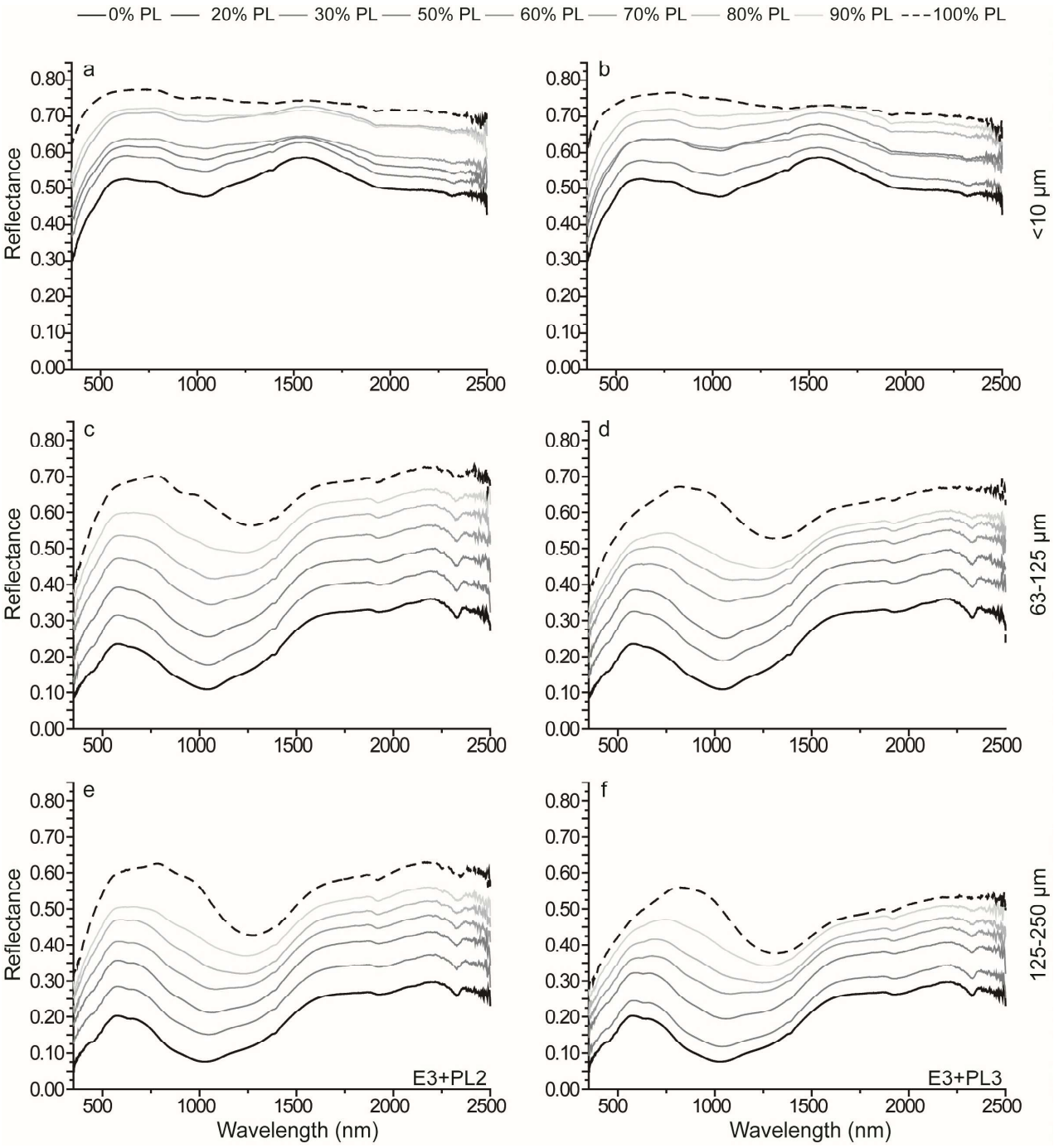
0% PL
20% PL
30% PL
50% PL
60% PL
70% PL
80% PL
90% PL
100% PL
a
b
c
d
e
f
Reflectance
Wavelength (nm)
<10 µm
63-125 µm
125-250 µm
E3+PL2
E3+PL3

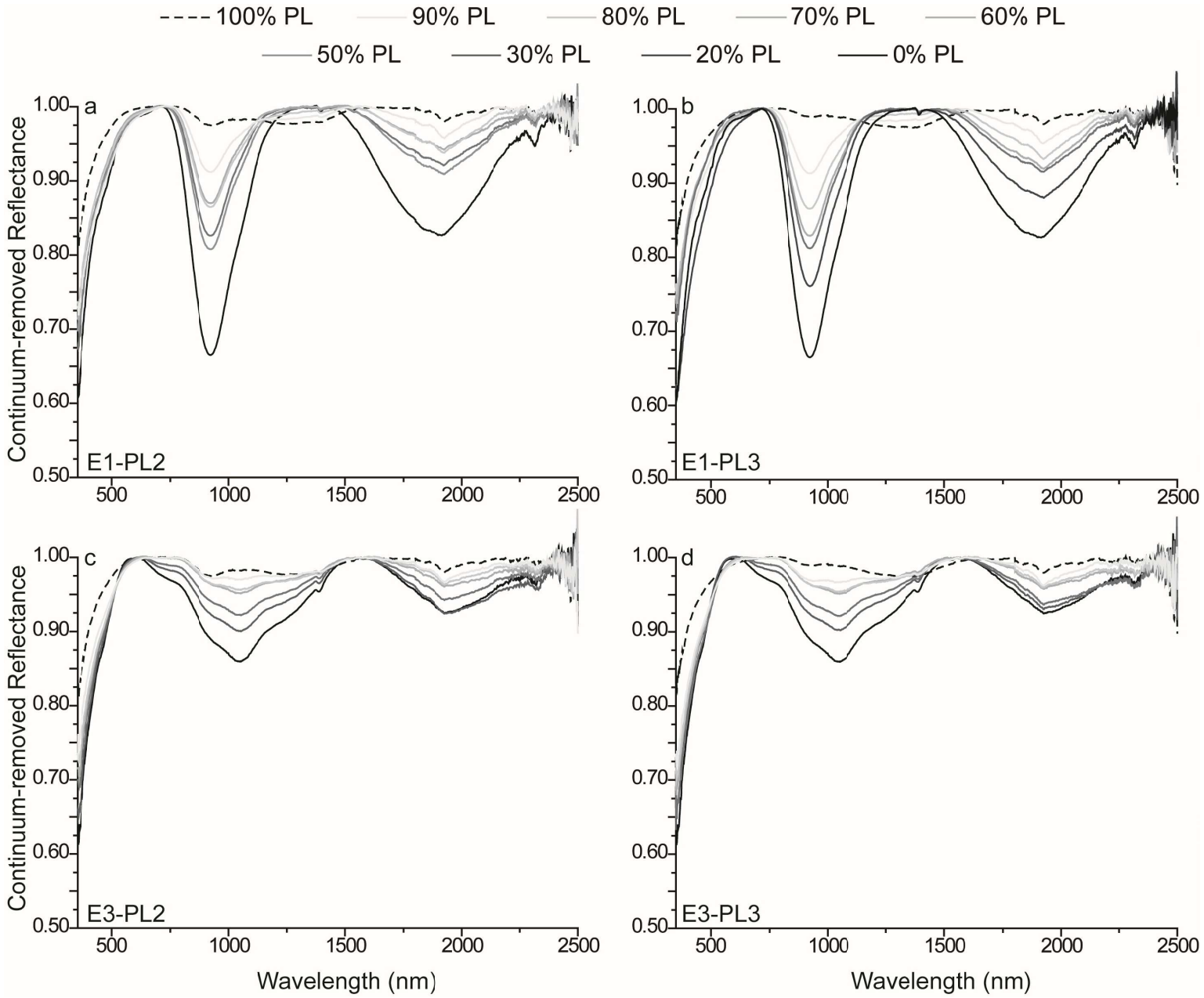
100% PL
90% PL
80% PL
70% PL
60% PL
50% PL
30% PL
20% PL
0% PL
a
b
c
d
E1-PL2
E1-PL3
E3-PL2
E3-PL3
Continuum-removed Reflectance
Wavelength (nm)
1.00
0.90
0.80
0.70
0.60
0.50
500
1000
1500
2000
2500

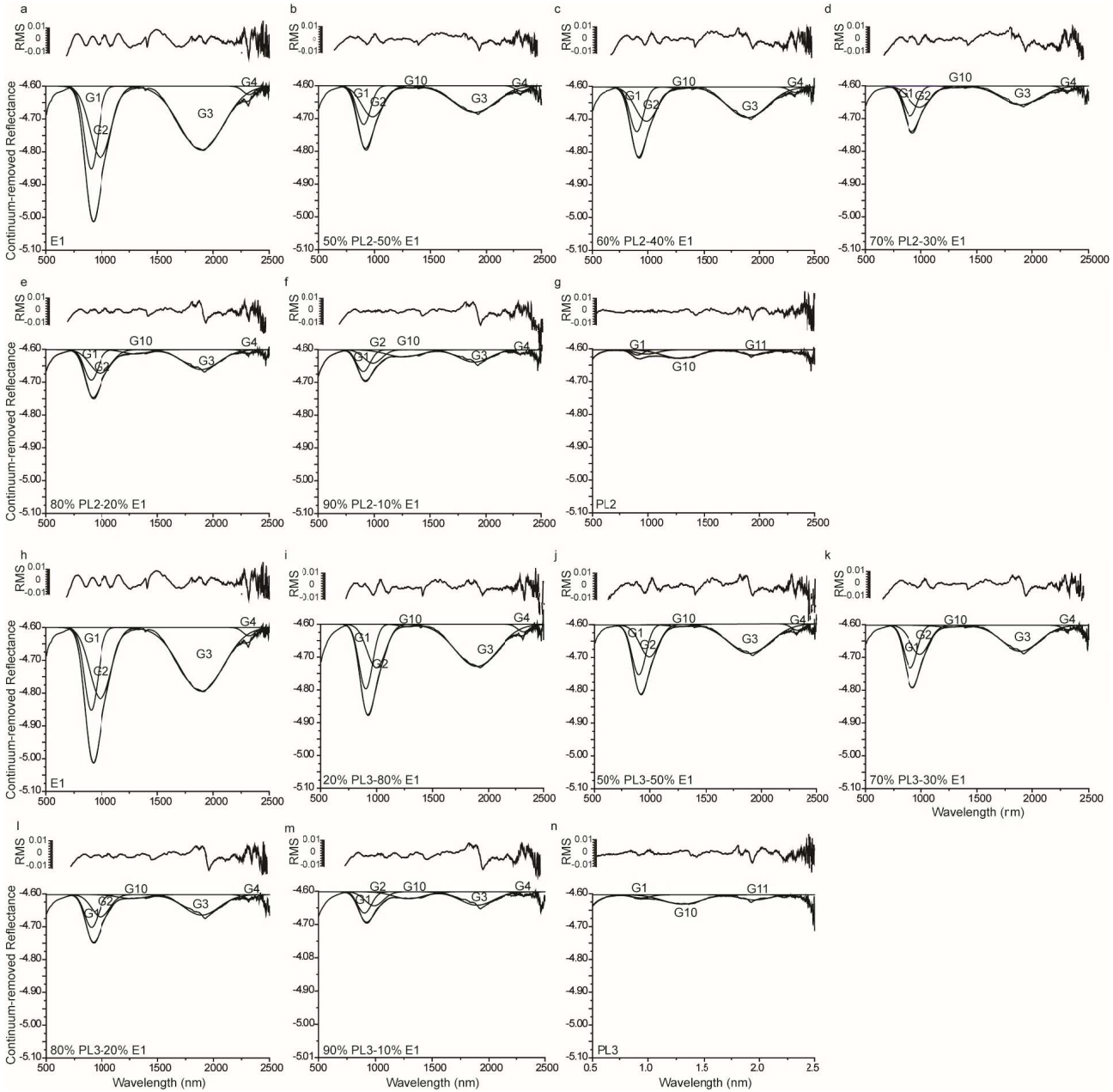
a
b
c
d
e
f
g
h
i
j
k
l
m
n
RMS
Continuum-removed Reflectance
G1
G2
G3
G4
G10
G11
E1
50% PL2-50% E1
60% PL2-40% E1
70% PL2-30% E1
80% PL2-20% E1
90% PL2-10% E1
PL2
20% PL3-80% E1
50% PL3-50% E1
70% PL3-30% E1
80% PL3-20% E1
90% PL3-10% E1
PL3
Wavelength (nm)
Wavelength (rm)

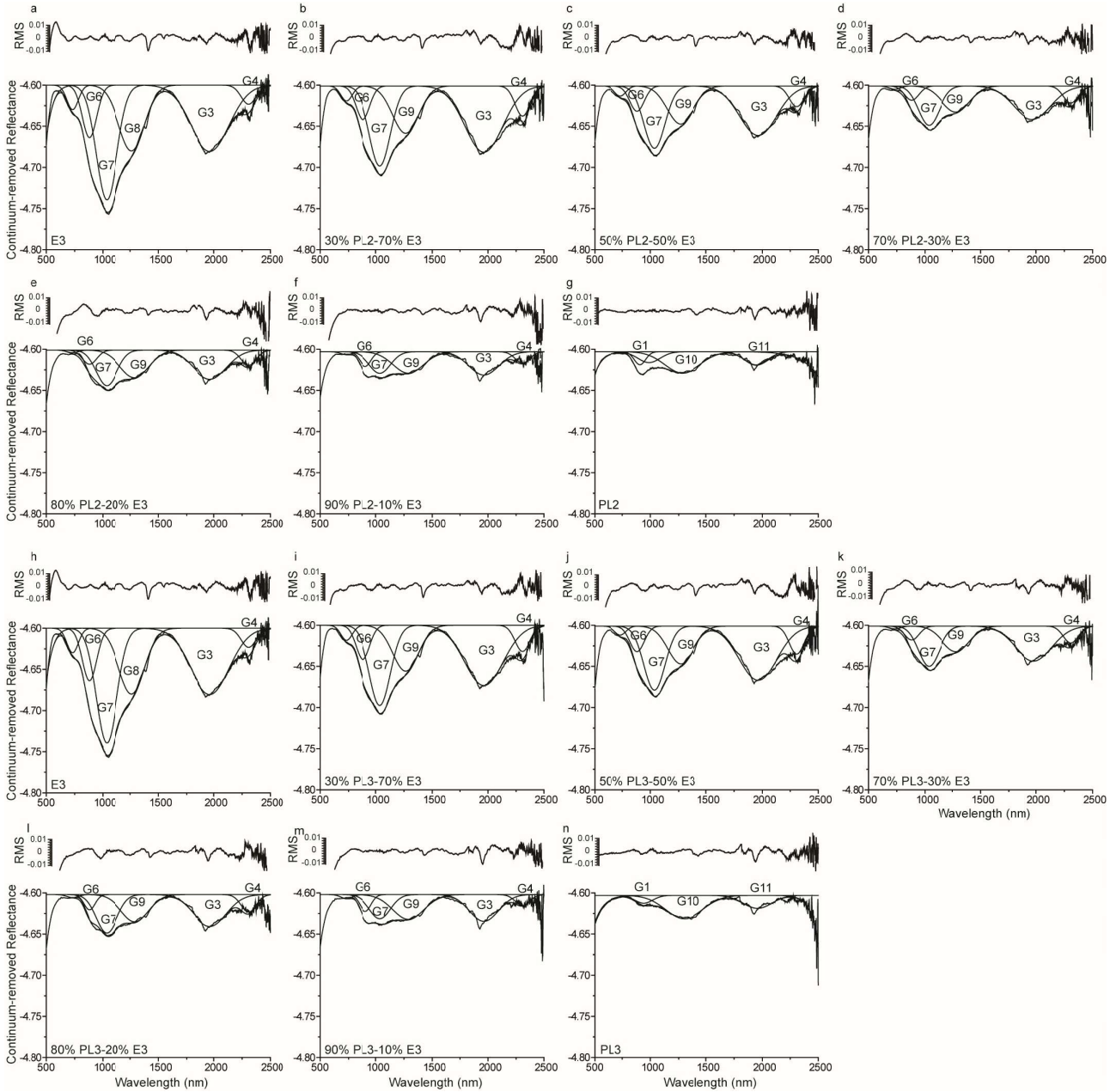
a
b
c
d
e
f
g
h
i
j
k
l
m
n
RMS
Continuum-removed Reflectance
Wavelength (nm)
E3
30% PL2-70% E3
50% PL2-50% E3
70% PL2-30% E3
80% PL2-20% E3
90% PL2-10% E3
PL2
30% PL3-70% E3
50% PL3-50% E3
70% PL3-30% E3
80% PL3-20% E3
90% PL3-10% E3
PL3
G1
G3
G4
G6
G7
G8
G9
G10
G11

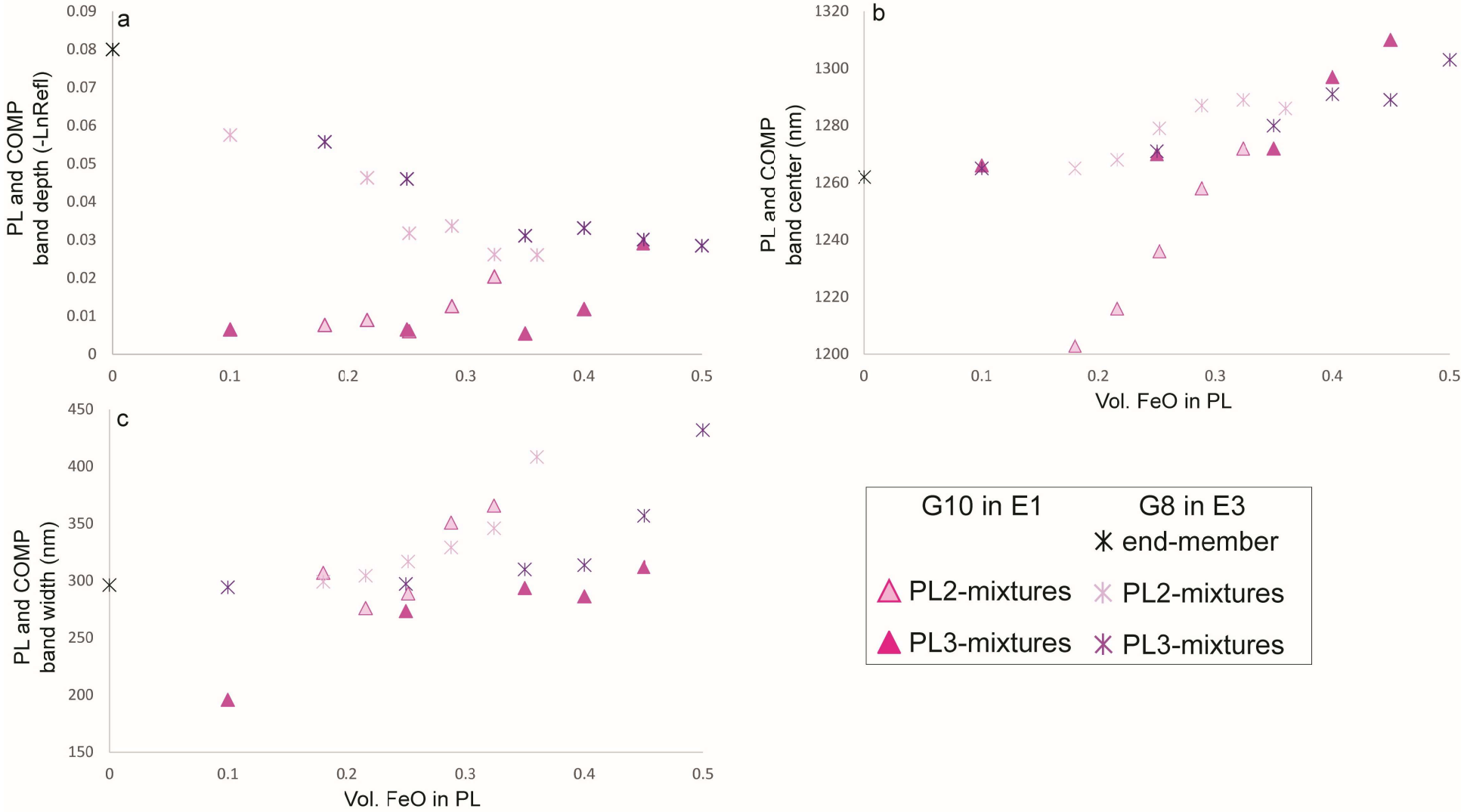
a
PL and COMP band depth (-LnRefl)
0.09
0.08
0.07
0.06
0.05
0.04
0.03
0.02
0.01
0
0
0.1
0.2
0.3
0.4
0.5
b
PL and COMP band center (nm)
1320
1300
1280
1260
1240
1220
1200
Vol. FeO in PL
c
PL and COMP band width (nm)
450
400
350
300
250
200
150
Vol. FeO in PL
G10 in E1
G8 in E3
end-member
PL2-mixtures
PL2-mixtures
PL3-mixtures
PL3-mixtures

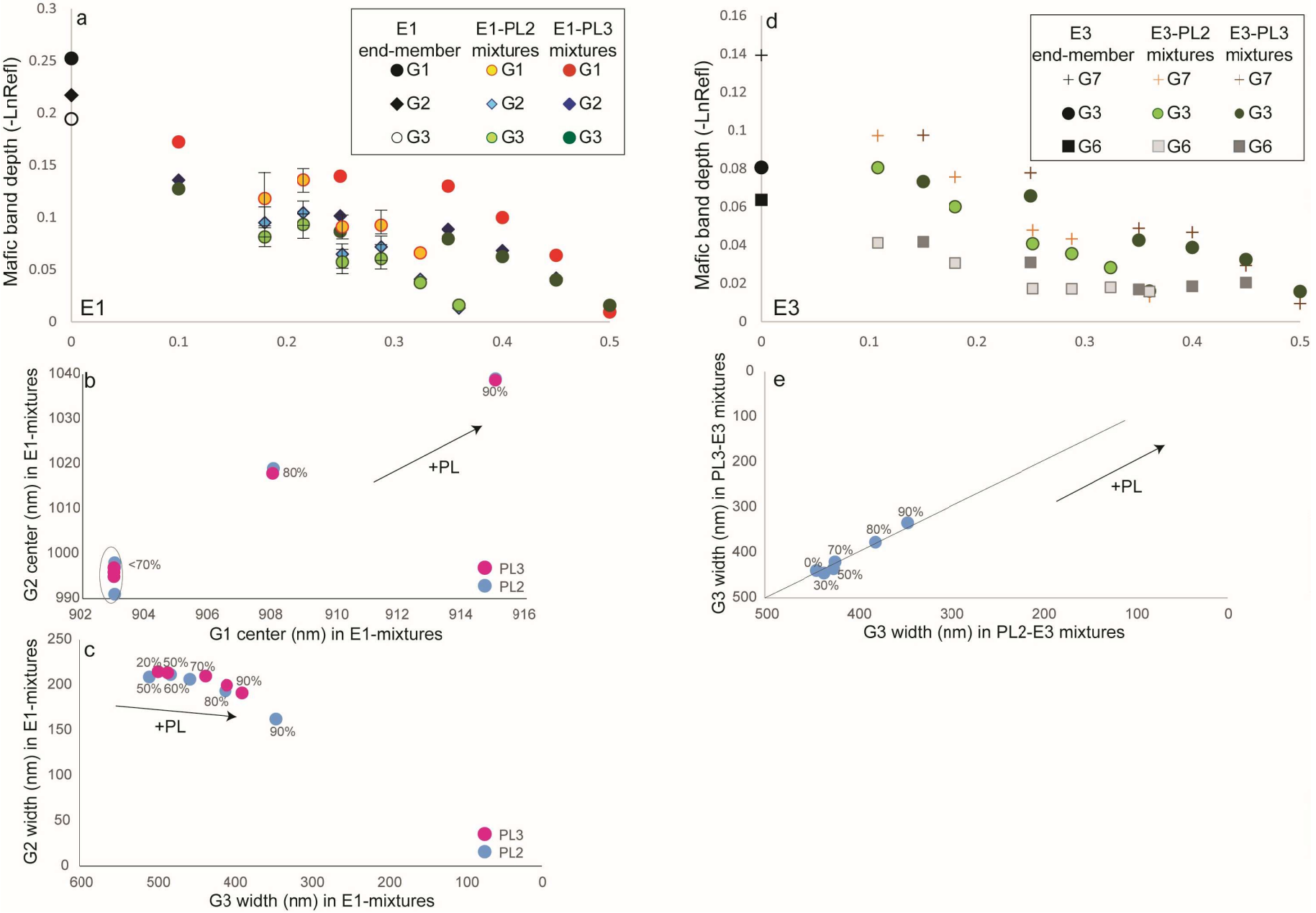
a
Mafic band depth (-LnRefl)
E1
E1 end-member
E1-PL2 mixtures
E1-PL3 mixtures
G1
G2
G3
b
G2 center (nm) in E1-mixtures
G1 center (nm) in E1-mixtures
90%
80%
<70%
+PL
PL3
PL2
c
G2 width (nm) in E1-mixtures
G3 width (nm) in E1-mixtures
20%
50%
70%
90%
80%
60%
+PL
d
Mafic band depth (-LnRefl)
E3
E3 end-member
E3-PL2 mixtures
E3-PL3 mixtures
G7
G3
G6
e
G3 width (nm) in PL3-E3 mixtures
G3 width (nm) in PL2-E3 mixtures
0%
30%
50%
70%
80%
90%
+PL

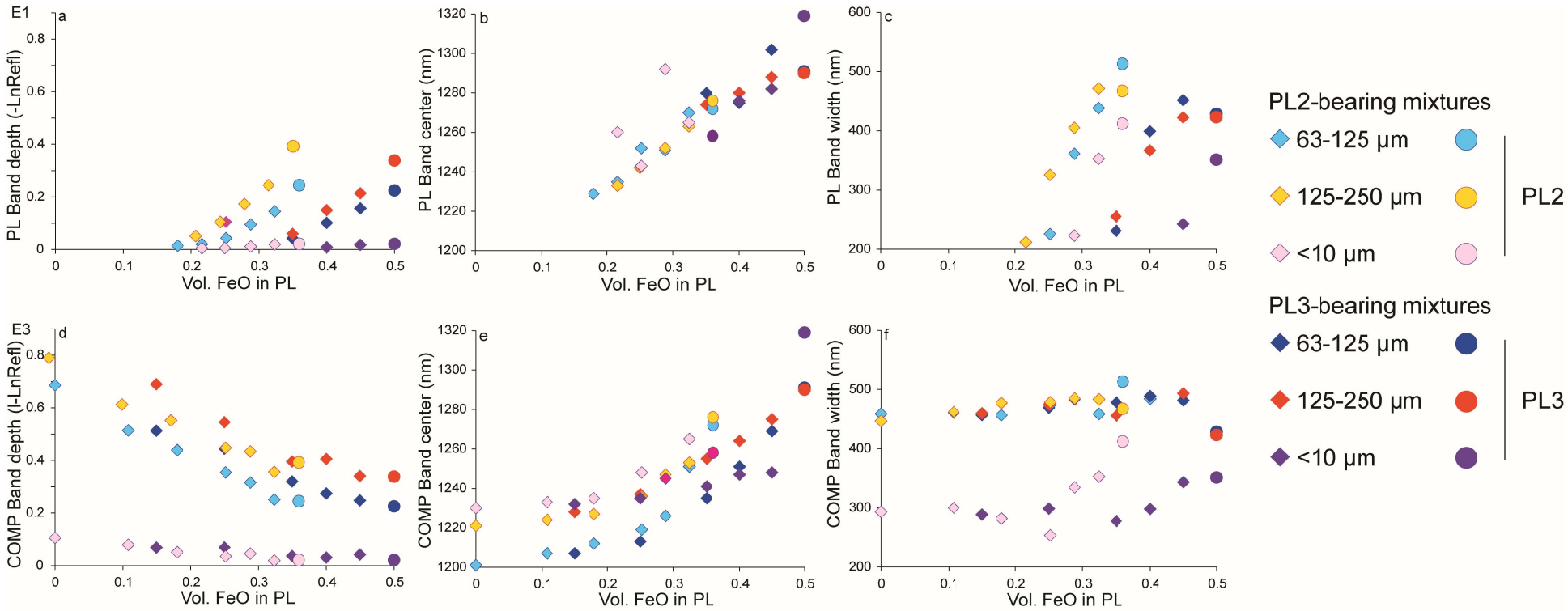
E1
a
PL Band depth (-LnRefl)
Vol. FeO in PL
b
PL Band center (nm)
Vol. FeO in PL
c
PL Band width (nm)
Vol. FeO in PL
E3
d
COMP Band depth (l-LnRefl)
Vol. FeO in PL
e
COMP Band center (nm)
Vol. FeO in PL
f
COMP Band width (nm)
Vol. FeO in PL
PL2-bearing mixtures
63-125 µm
125-250 µm
<10 µm
PL2
PL3-bearing mixtures
63-125 µm
125-250 µm
<10 µm
PL3

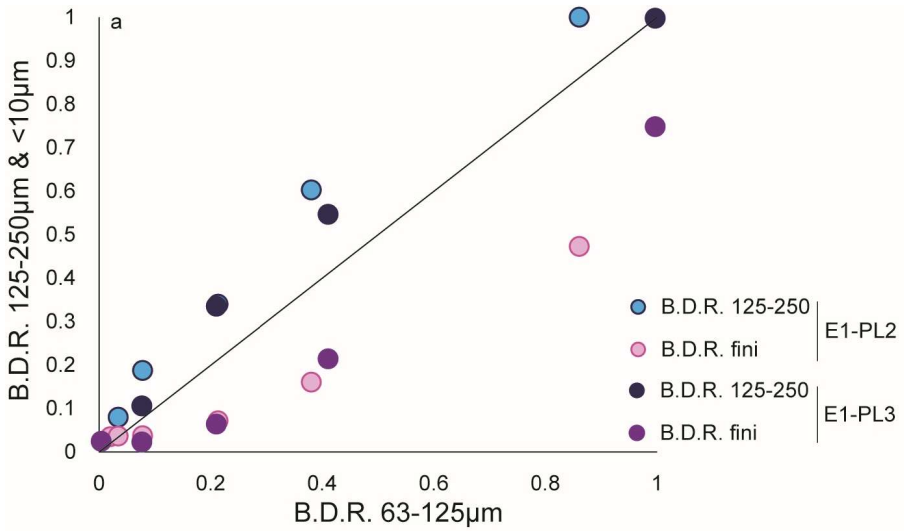
a
B.D.R. 125-250µm & <10µm
B.D.R. 63-125µm
0
0.1
0.2
0.3
0.4
0.5
0.6
0.7
0.8
0.9
1
0.2
0.4
0.6
0.8
B.D.R. 125-250
B.D.R. fini
E1-PL2
B.D.R. 125-250
B.D.R. fini
E1-PL3

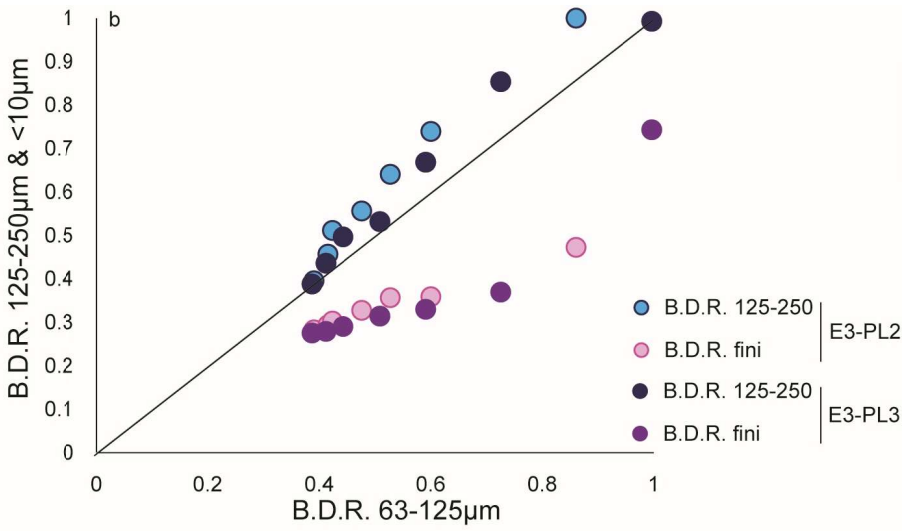
b
B.D.R. 125-250µm & <10µm
B.D.R. 63-125µm
0
0.1
0.2
0.3
0.4
0.5
0.6
0.7
0.8
0.9
1
0.2
0.4
0.6
0.8
B.D.R. 125-250
B.D.R. fini
E3-PL2
B.D.R. 125-250
B.D.R. fini
E3-PL3

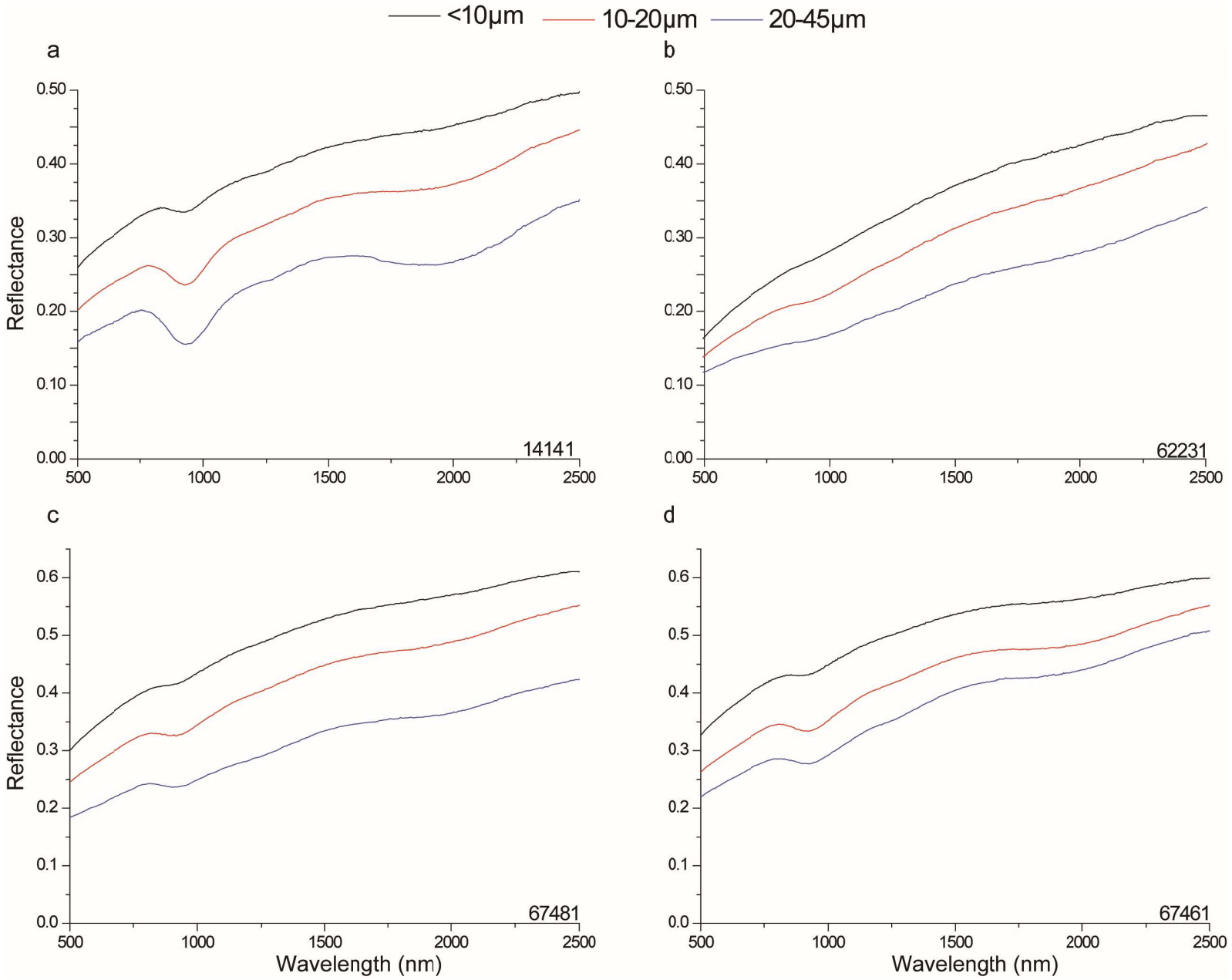
<10μm
10-20μm
20-45μm
a
b
c
d
Reflectance
Wavelength (nm)
14141
62231
67481
67461

Lithology	Mineral Abundance						Amp.	Minerals removed	New samples	Chemistry	FeO wt.%
	OPX %	CPX %	OL %	PL %	Op %	FeO wt. %					
Ultramafic rock	47	-	19.7	5.1	28.3	FeO wt. %	0.3 1.4	Op PL	CPX+OPX+OL(E3)	OPX(28.2%) En_{82}-Wo_4 CPX(3.4%) En_{45}-Wo_{46} OL(68.4%) Fo_{84}	9.03 3.8 14.65
Anorthosite	0.8	4.3	-	94.2	-	FeO wt. %	1.4	CPX+OPX+Zois.	PL(PL3)	PL3 An_{80}	0.36
Gabbronorite	22.1	17.3	-	60.6	-	FeO wt. %	1.4	None	CPX+OPX(E1) PL(PL2)	CPX(43.9%) En_{45}-Wo_{46} PL2 An_{80} OPX(56.1%) En_{77}-Wo_2	5.72 0.5 13.45

Tab. 1 Mineral abundances in the starting samples. OPX=orthopyroxene; CPX=clinopyroxene; OL=olivine; PL=plagioclase; Op=opaque minerals; Zois=zoisite. Table also shows the applied amperage (Amp.), the minerals removed and the final samples obtained with the Frantz Isodynamic Magnetic Separator. Chemistry and iron abundance of the new samples are also reported.

Gaussian	Position (nm)	Interpretation
G1	900-950	Fe^{2+} in OPX M2 site
G2	1000-1100	Fe^{2+} in CPX M2 site
G3	1850-2000	Fe^{2+} in OPX M2 site/ chromite
G4	2200-2300	Fe^{2+} in CPX M2 site/ Al-OH alterations
G5	840	Adjustment Gaussian
G6	850-950	Fe^{2+} in OL M1 site
G7	1000-1100	Fe^{2+} in OL M2 site
G8	1200-1250	Fe^{2+} in OL M1 site
G9	1200-1300	COMP band (Fe^{2+} in OL M1 site+Fe^{2+} in PL)
G10	1250-1300	Fe^{2+} in PL
G11	1600-1800	PL asymmetry/PL alteration

Tab. 2 In the table are reported a list of Gaussians used in the end-member deconvolution, the wavelength position and the mineralogical interpretation.

	E1											
	63-125 µm				125-250 µm				<10 µm			
	Center	Width	Depth	RMS	Center	Width	Depth	RMS	Center	Width	Depth	RMS
G5	843±9	110	-0.400		837±6	113	-0.370					
G1	934±9	159	-0.929		949±30	180	-0.895		903±10	154	-0.252	
G2	1028±20	199	-0.535		1058±30	191	-0.371		988±10	220	-0.217	
G3	1851±11	496	-0.766		1813±15	489	-0.631		1894±10	509	-0.194	
G4	2311±50	730	-0.431		2202±50	678	-0.586		2321±40	138	-0.025	
				0.018				0.020				0.06
	E3											
	63-125 µm				125-250 µm				<10 µm			
	Center	Width	Depth	RMS	Center	Width	Depth	RMS	Center	Width	Depth	RMS
G6	861±7	210	-0.464		842±2	193	-0.483		881±10	163	-0.063	
G7	1028±6	204	-0.562		1009±2	218	-0.722		1036±8	241	-0.139	
G8	1221±3	400	-0.655		1221±2	408	-0.789		1262±10	296	-0.08	
G3									1963±2	442	-0.080	
				0.005				0.003				0.005

Tab. 3 In table are reported the spectral parameters obtained by MGM deconvolution of mafic end-members, at the 63-125µm (on the left), 125-250µm (on the central column) and <10 µm (on the right). Center and width are expressed in nanometers, while depth as the logarithm of the reflectance. RMS represents the Root Mean Square error: the lower the RMS the better the fit. To show the goodness of the fit, for band center, the error calculated at 95% level of confidence was reported.

	PL2											
	63-125 µm				125-250 µm				<10 µm			
	Center	Width	Depth	RMS	Center	Width	Depth	RMS	Center	Width	Depth	RMS
G10	1271±1	505	-0.2439		1282±1	481	-0.3919		1286±6	408	-0.026	
G11	1837±6	443	-0.04704		1822±6	441	-0.06778		1944±4	250	-0.016	
G1	909±2	122	-0.0395		881±1	54	-0.0097		907±3	129	-0.015	
				0.005				0.009				0.003

	PL3											
	63-125 µm				125-250 µm				<10 µm			
	Center	Width	Depth	RMS	Center	Width	Depth	RMS	Center	Width	Depth	RMS
G10	1298±2	438	-0.2356		1295±2	431	-0.3598		1303±5	432	-0.028	
G11	1734±12	591	-0.06649		1711±13	636	-0.1066		1957±6	325	-0.016	
G1									941±4	205	-0.01	
				0.005				0.007				0.003

Tab. 4 In table are reported the spectral parameters obtained by MGM deconvolution of mafic end-members, at the 63-125µm (on the left), 125-250µm (on the central column) and <10 µm (on the right). Center and width are expressed in nanometers, while depth as the logarithm of the reflectance. RMS represents the Root Mean Square error: the lower the RMS the better the fit. To show the goodness of the fit, for band center, the error calculated at 95% level of confidence was reported.

1) 5-20% of lunar regolith is very fine grained (<10μm)
2) Very fine sizes increase the albedo but reduce the spectral contrast
3) Very fine plagioclase has featureless spectrum
4) Mafic materials are affected by fine sizes